

**Nanoparticle Adsorption Dynamics at Fluid Interfaces**

Journal:	<i>Soft Matter</i>
Manuscript ID	SM-ART-02-2018-000273.R1
Article Type:	Paper
Date Submitted by the Author:	10-Apr-2018
Complete List of Authors:	Hua, Xiaoqing; Johns Hopkins University Frechette, Joelle; Johns Hopkins University, Chemical and Biomolecular Engineering Bevan, Michael; Johns Hopkins University,

Nanoparticle Adsorption Dynamics at Fluid Interfaces

Xiaoqing Hua, Joelle Frechette, and Michael Bevan**

Chemical and Biomolecular Engineering, Johns Hopkins University, Baltimore, MD 21218

Email: mabevan@jhu.edu, jfrechette@jhu.edu

ABSTRACT

Understanding the dynamic adsorption of nanoparticles (NPs) at fluid interfaces is important for stabilizing emulsions and for the preparation of 2D NPs-based materials. Here we show that the Ward-Tordai equations commonly employed to describe the dynamic of surfactant adsorption at a fluid interface combined with a Frumkin adsorption isotherm can be employed to model the diffusion-limited adsorption of NPs onto a fluid interface. In contrast to surfactants, an additional wetting equation of state (EOS) must be incorporated to characterize the dynamic interfacial tension during the adsorption of NPs to the oil-water interface. Our results show agreement between the model and experiments at NP area fraction < 0.3 . Slower dynamics are observed at larger area fractions, which are speculated to arise from polydispersity or re-organization at the interface. We show the model can be extended to the competitive adsorption between the NPs and a surface active species.

Introduction

Adsorption of particles or nanoparticles (NPs) decreases the interfacial tension of a fluid interface and leads to the stabilization of foams and emulsions.¹⁻³ Particle-laden fluid interfaces have received attention for their applications in catalysis,^{4, 5} sensing,^{6, 7} and optics.^{8, 9} As a particle adsorbs, oil-water interfacial area is replaced by particle-fluid interfaces. This area replacement causes a decrease of the free energy of the interface, ΔE , (per particle) given by Eqn. (1):¹⁰

$$\Delta E = -\pi r_{NP}^2 \gamma_{OW} (1 \pm \cos \theta_{OW})^2, \quad (1)$$

where r_{NP} is the radius of the NP, γ_{OW} is the oil-water interfacial tension, and θ_{OW} is the contact angle formed by the NP at the oil-water interface.

The decrease in interfacial tension (IFT) caused by the adsorption of a species to a fluid interface is a macroscopic mechanical response that is easily accessible experimentally. For surfactants, the IFT can be employed in conjunction with the Gibbs adsorption isotherm to determine the adsorbed amount when equilibrium is established between the bulk and the interface.¹¹ In the case of particle adsorption, steady-state IFT measurements have been employed to test the applicability of Eqn. (1).^{12, 13} Similarly, dynamic IFT measurements allow for the characterization of mass transfer and adsorption processes. In the case of surfactants, analysis and interpretation of dynamic IFT measurements have been employed to explain induction times,^{14, 15} extract energy barrier,^{16, 17} study interfacial phase transitions during adsorption,^{14, 18} and to validate adsorption isotherms and surface equations of state¹¹. However, unlike surfactants, there are no validated models for the diffusion-limited adsorption of particles to fluid interfaces. Despite the importance of particle-laden interfaces, the dynamic of their adsorption and its impact on interfacial tension remains poorly understood.^{19, 20} For example, Colosqui *et al.*²¹ has shown that the particle surface heterogeneities may result in physical aging and jamming, giving rise to unexpected long relaxation.

Understanding how particle adsorption influences dynamic IFT has proven to be challenging. Due to their relatively larger sizes compared to surfactants, particles have a smaller diffusivity that slows adsorption and, as a result, dynamic IFT measurements are more susceptible to convection and contamination. In addition, the large adsorption energy given by Eqn. (1) often makes the adsorption process irreversible, rendering data interpretation more challenging.^{19, 22}

Moreover, there is evidence that in some instances adsorbed particles form multilayers or even aggregates at the interface.^{23, 24} Finally, there has been limited characterization of equilibrium particle adsorption at oil-water interfaces.^{25, 26} In particular, adsorption isotherms and EOS are necessary to model the dynamic interfacial tension, and those are often lacking for particle adsorption to fluid interfaces. Despite these challenges, efforts to model the dynamic IFT have clearly demonstrated that the diffusion-limited adsorption of particles is quantitatively different from that of surfactants.^{19, 27, 28} In particular, the asymptotic behaviors (the dynamic IFT at short and long times) derived for surfactant adsorption^{29, 30} are not applicable without modifications for NP adsorption.

Efforts to model the dynamic IFT have been centered on obtaining asymptotic limits for the dynamic IFT that are applicable to the adsorption of NPs at a fluid interface. Recently, Bizmark *et al.*¹⁹ proposed relationships for both short- and long-time limits. For the short-time limit they described the adsorption process as being diffusion-limited and corrected the form available for surfactant for particle wetting using Eqn. (1). Their asymptotic limit at short-time showed good agreement with experimental measurements. For the long-time limit Bizmark *et al.*¹⁹ argued that the adsorption of NPs was no longer diffusion-limited and was irreversible. Based on these assumptions, they derived a long-time asymptotic for the dynamic interfacial tension based on random sequential adsorption (RSA). However, whether or not their measurements were in the diffusion-limited regime was not determined. The model was employed to extract an energy barrier for NP adsorption, and later used by Nelson *et al.*³¹ to extract the adsorption energy. To apply the RSA model, the area fraction of adsorbed NPs is assumed to be the hard disk limit (0.907) independent of bulk concentration,^{19, 31} which is larger than the RSA saturation density of hard disks (0.547).³² In addition, multiple literature reports indicate an adsorbed amount of NPs that is dependent on their bulk concentrations (partitioning between the bulk and the interface).^{25, 26, 33} Moreover, for both the long- and short-time limits, the asymptotic slopes of the dynamic IFT are usually small, often comparable or even smaller than the resolution of the measurements.^{19, 29, 31} Therefore there is a need to develop a full model (along with the associated long-time limit) for diffusion-limited NP adsorption that can be validated experimentally. Such a model would be helpful to determine the rate-limiting step, and to demonstrate evidence of kinetic limitations in the adsorption process. An additional challenge in testing dynamic IFT model for NP adsorption is that the surface coverage is usually not

measured independently, making it difficult to validate the dynamic model when equilibrium parameters are also obtained from the dynamic IFT as well.

Previously, we reported on the reversible adsorption of 5 nm and 10 nm gold NPs functionalized with ion-pair ligands (Figure 1 left panel).^{26, 34} Based on independently measured pressure and adsorption isotherms, we constructed the equation of state (EOS) for the particles at the oil-water interface. We showed that the adsorption isotherm was well-described by the Frumkin isotherm, while the surface pressure measured in the EOS had two contributions: one originating from the wetting of the NPs to the oil-water interface and the other from the surface activity of the NPs at the oil-water interface. We showed that the contribution from surface activity on the surface pressure was much weaker compared to that of wetting, and in most cases could safely be neglected. However, the dynamics of the diffusion-limited NP adsorption to the oil-water interface was not characterized and compared to a mass transfer model, such as the Ward-Tordai equations used for surfactant adsorption.

Here we show that the Ward-Tordai equations can fully describe the dynamic IFT for 5 nm and 10 nm ion-pair NPs at the water-toluene interface, with equilibrium parameters obtained from independent measurements of the adsorption isotherm.^{26, 35} We show that the Ward-Tordai equations, when combined with the equilibrium model developed previously, lead to good agreement between data and experiments for the whole adsorption process. We also observe deviations between the model and experiments at high surface coverage that could be attributed to polydispersity or other kinetic limitations. Finally, we also show that our model can qualitatively capture the competitive adsorption between NPs and a surfactant for the oil-water interface. To the best of the authors' knowledge, the data presented here is the first direct test of a measurement and model for the diffusion-limited adsorption of NPs to the oil-water interface.

Diffusion-limited adsorption model

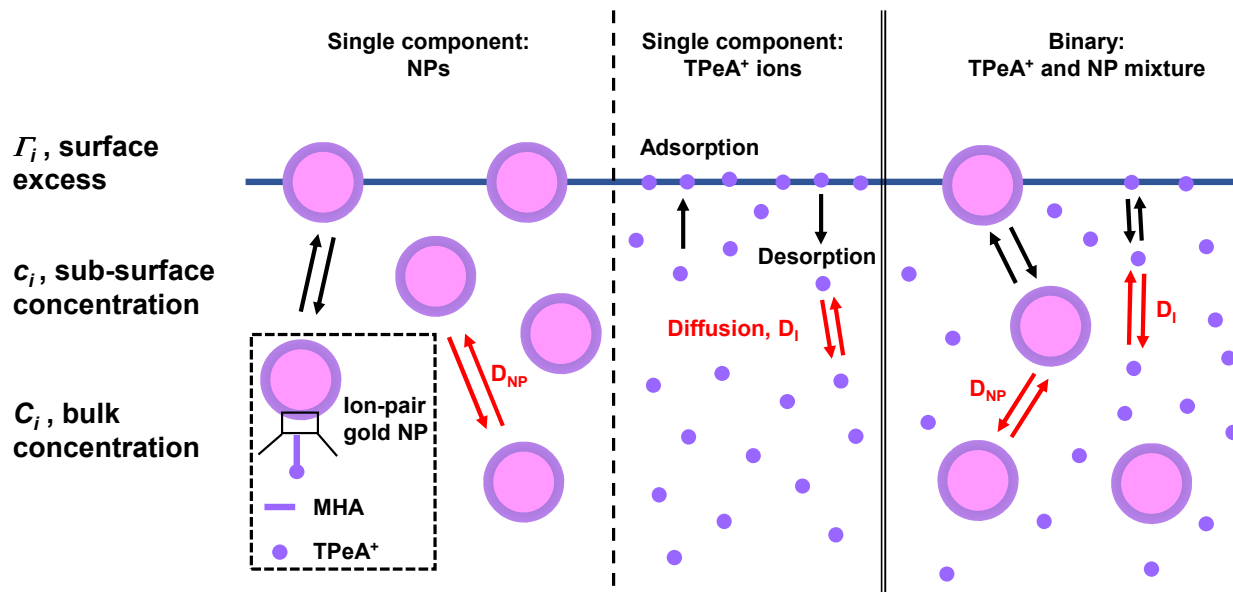


Figure 1. Schematic of adsorption dynamics illustrating the two primary steps governing the mass transfer to the interface: 1) the adsorption (black up arrows) and desorption (black down arrows) between the sub-surface region and the interface, as well as 2) the diffusion (red arrows) from bulk phase to the sub-surface. The processes are shown for single components (NPs, left panel, and TPEA⁺ ion, middle panel) and for a binary mixture (NPs-TPEA mixture, right panel).

Ward-Tordai model

The adsorption process in the Ward-Tordai model (Eqn. (2)), originally developed for surfactant adsorption to a clean interface is governed by two primary steps: 1) the diffusion of the species from the bulk phase to the sub-surface, followed by 2) the adsorption from the sub-surface region onto the interface, as illustrated in (Figure 1).³⁶ In the case of diffusion-limited adsorption, it is assumed that instantaneous equilibrium is established between the surface excess at the interface (Γ_i) and the concentration in the sub-surface region (c_i).²² Thus the rate of adsorption is limited by the diffusion from the bulk phase to the sub-surface region, which can be described by Fick's law. The solution of the Ward-Tordai model (Eqn. (2)) has been employed to capture the diffusion-limited adsorption of various surfactants^{37, 38} and macromolecules^{39, 40}. Due to near-spherical shape in pendant drop measurements, we rely on the formulation of Lin *et al.* in spherical coordinates given by:⁴¹

$$\Gamma_i(t) = \sqrt{\frac{D_i}{\pi}} \left\{ 2C_i\sqrt{t} - \int_0^t \frac{c_i(\tau)}{\sqrt{t-\tau}} d\tau \right\} + \frac{D_i}{r_D} \left\{ C_i t - \int_0^t c_i(\tau) d\tau \right\}, \quad (2)$$

where i is the surface active species (NPs for example), C_i is the bulk concentration of the adsorbing species, r_D is the radius of the pendent droplet. D_i is the diffusivity of the adsorbing species, which can be estimated using Stokes-Einstein equation:⁴²

$$D_{i-SE} = \frac{kT}{6\pi\mu r_i}, \quad (3)$$

where D_{i-SE} specifically refers to the diffusivity predicted using Eqn. (3), k is the Boltzmann constant, T is temperature, μ is the fluid viscosity, and r_i is the radius of the surface active species, here referring to NP for example (Figure 1).

Single component adsorption

In diffusion-limited adsorption, instantaneous equilibrium is established between the sub-surface and the interface. The time-dependent surface coverage, $\Gamma_i(t)$, can be related to the sub-surface concentration, $c_i(t)$ through an adsorption isotherm. Here we employ the Frumkin adsorption isotherm, which incorporates non-ideal interactions between adsorbed species within the interface^{37, 43}, and describes well the adsorption of the NPs investigated here⁴³ as well as surfactants at oil-water interfaces, and is given by:

$$c_i(t) = a_{L,i} \frac{\theta_i(t)}{1 - \theta_i(t)} \exp[K_i \theta_i(t)], \quad (4)$$

where i is the adsorbed species (NPs for example), $\theta_i(t) = \Gamma_i(t) / \Gamma_{i,\infty}$ is the transient relative coverage of the surface-active species i at the interface at time t , and $\Gamma_{i,\infty}$ is the maximum surface excess of i . The affinity between the surface active species and the interface is captured by the dissociation constant, $a_{L,i}$, while the parameter K_i accounts for the interactions between the species i within the interface relative to the thermal energy, kT ,⁴⁴ where a positive value represents net repulsion, and a negative value represents attractive interactions.⁴⁵

The integration of the Ward-Tordai equation combined with the Frumkin adsorption isotherm (Eqns. (2)-(4)) results in dynamic surface excess, which is not easily accessible experimentally. Therefore, an EOS is necessary to relate the surface excess to a measurable dynamic IFT. The corresponding Frumkin EOS, that is thermodynamically consistent with the Frumkin adsorption isotherm following the Gibbs adsorption criteria,^{46, 47} dictates the contribution from surface activity of NPs (Π_{SA}), to be^{37, 43}:

$$\Pi_{SA} = -kT\Gamma_{i,\infty} \left[\ln(1-\theta_i) - 0.5K_i\theta_i^2 \right] . \quad (5)$$

The thermodynamic parameters (parameters in Eqns. (4)-(5)) associated with description of equilibrium adsorption behavior can be obtained via fitting to equilibrium data (pressure isotherm or adsorption isotherm).²⁶

Wetting EOS for NP adsorption

Measured surface pressures caused by NP adsorption are often much larger than those predicted by the Frumkin EOS.^{13,26,28} The main contribution to the surface pressure is that of the wetting of the NPs at the liquid-liquid interface, as fluid-fluid area is replaced by particle-fluid area.¹⁰ Du *et al.* proposed that the surface pressure (Π_{NP}) originating from this area replacement process is given by¹²:

$$\Pi_{NP} = |\Delta E| \times \Gamma_{NP} , \quad (6)$$

where Γ_{NP} is the surface coverage of NP at oil-water interface, and ΔE is the adsorption energy of a single NP given by Eqn. (1).

We suggested previously that the measured surface pressure originates from both the surface activity (Eqn. (5)) and wetting (Eqn. (6)) of the NPs, and validated this hypothesis through measurements of equilibrium pressure and adsorption isotherms.³⁵ We proposed that the two contributions could be treated as additive, however in most scenarios the contribution from surface activity can be neglected. As a result, the transient reduction in interfacial tension when incorporating these contributions will be given by:

$$\gamma(t) = \gamma_{OW} - \Pi_{SA}(t) - \Pi_{NP}(t) . \quad (7)$$

Therefore, prediction for the dynamic IFT due to diffusion-limited adsorption of NPs to an oil-water interface can be obtained by solving Eqns. (2)-(7). Note here that this approach is different from surfactant adsorption, where surface activity is the only contribution to the measured IFT.

Asymptotic limits

Based on the model described in Eqns. (2)-(7) we can derive the asymptotic limits for the dynamic IFT for NP adsorption at both short- and long-times. In the short-time limit, as $t \rightarrow 0$ (< 1 second for surfactants,²⁹ < 20 seconds for particles¹⁹), Eqn. (2) can be simplified to³⁰:

$$\Gamma_i(t) = 2C_i \sqrt{\frac{D_i t}{\pi}}. \quad (8)$$

For NP adsorption, the wetting EOS (Eqn. (6)) can be combined with Eqn. (8) to obtain the short-time limit, resulting in the same equation as Bizmark *et al.*,¹⁹ given by:

$$\gamma = \gamma_{OW} - 2|\Delta E|C_{NP} \sqrt{\frac{D_{NP} t}{\pi}}. \quad (9)$$

For the long-time limit, when $t \rightarrow \infty$, the subsurface concentration, c_i , approaches the bulk concentration, C_i . As a result, the following difference between bulk concentration and subsurface concentration can be obtained²⁹:

$$\Delta c = C_i - c_i = \Gamma_i \sqrt{\frac{\pi}{4D_i t}}. \quad (10)$$

Following the procedure for asymptotes of surfactants,²⁹ followed by incorporating the wetting EOS (Eqn. (6)) and the Frumkin adsorption isotherm (Eqn. (4)) into Eqn. (10), the long-time limit for particle adsorption is given by (with additional details provided in supporting information):

$$\gamma = \gamma_{eq} + (|\Delta E|) \left(\frac{1 - \theta_{NP}}{1 + K_{NP} \theta_{NP} (1 - \theta_{NP})} \right) \left(\frac{\Gamma_{NP}^2}{C_{NP}} \sqrt{\frac{\pi}{4D_{NP} t}} \right), \quad (11)$$

where γ_{eq} is the equilibrium interfacial tension corresponding to the bulk concentration C_{NP} . The long-time limit for particle adsorption consists of three contributions bracketed on the right-hand-side of Eqn. (11). The last bracketed term is the same as the one obtained for surfactant adsorption.²⁹ The first term accounts for the wetting contribution during particle adsorption (*i.e.*, $|\Delta E|$ in Eqn. (1)). Finally, the middle-bracketed term in Eqn. (11) is a contribution from the adsorption isotherm. This middle term has an upper bound of 1 when $\theta_{NP} \rightarrow 0$, and a lower bound of 0 when $\theta_{NP} \rightarrow 1$. Note that as $\theta_{NP} \rightarrow 1$ the bulk NP concentration is sufficiently large that the surface coverage reaches equilibrium before equilibrium between the sub-surface and bulk concentrations.²² Thus the long-time limit analysis is not valid under these conditions. When the NP-NP interaction parameter is negligible, *i.e.* $K_{NP} \approx 0$, the long-time limit reduces to the one obtained from Langmuir adsorption isotherm, given by:

$$\gamma = \gamma_{eq} + |\Delta E| \frac{(1 - \theta_{NP}) \Gamma_{NP}^2}{C_{NP}} \sqrt{\frac{\pi}{4D_{NP}t}}. \quad (12)$$

The long-time limit obtained by combining wetting EOS and adsorption isotherm, takes into account both C_{NP} , the relative surface coverage, θ_{NP} , and particle-particle interaction, K_{NP} . It is different from the result obtained based on RSA from Bizmark *et al.*¹⁹ where the long-time limit is independent of relative coverage, but depends on a blocking function based on irreversible and laterally immobile particles.

In contrast to similar measurements performed to characterized surfactant adsorption,²⁹ the change in the dynamic IFT in the short-time limit is very small ($d\gamma(t)/dt^{1/2} \rightarrow 0$), which can lead to a large error when adsorption energy is to be extracted from the short-time limit. Similarly, in the slope for long-time limit ($d\gamma(t)/dt^{-1/2}$) can also be close to 0, resulting in unreliable interpretation.

Binary adsorption

We also extend the model to the case of competitive adsorption between NPs and surfactants. Thus, a binary Frumkin model⁴⁸ is employed to describe the adsorption isotherms for the two species (NPs and surfactant), which includes the interactions between individual species (K_{NP} , K_I) and between different species (*i.e.*, NP-ion interactions, K_{NP-I}). The corresponding isotherms that captures the instantaneous equilibrium between surface coverage ($\Gamma_i(t)$) and sub-surface concentration ($c_i(t)$) of the two species are given by^{40, 48}:

$$c_I(t) = a_{L,I} \frac{\theta_I(t)}{1 - \theta_I(t) - \theta_{NP}(t)} \exp[K_I \theta_I(t) + K_{NP-I} \theta_{NP}(t)], \quad (13)$$

$$c_{NP}(t) = a_{L,NP} \frac{\theta_{NP}(t)}{1 - \theta_{NP}(t) - \theta_I(t)} \exp[K_{NP} \theta_{NP}(t) + K_{NP-I} \theta_I(t)]. \quad (14)$$

The corresponding binary EOS related to the binary Frumkin adsorption isotherms is:^{40, 48}

$$\Pi_{Bin} = -kT\Gamma_\infty \left[\ln(1 - \theta_I - \theta_{NP}) - 0.5K_I \theta_I^2 - 0.5K_{NP} \theta_{NP}^2 - K_{NP-I} \theta_I \theta_{NP} \right], \quad (15)$$

where $\Gamma_\infty = (\Gamma_I + \Gamma_{NP}) / (\theta_I + \theta_{NP})$ is the total surface coverage, allowing for different maximum coverage for each of the individual components.⁴⁸

Similar to our approach for NP adsorption, we propose that two contributions (surface activity and wetting of the interface) cause a reduction of the interfacial tension. By adding the two contributions, the instantaneous reduction of the IFT is:

$$\gamma(t) = \gamma_{OW} - \Pi_{Bin}(t) - \Pi_{NP}(t) . \quad (16)$$

Thus the diffusion-limited adsorption in the case of competitive adsorption is obtained by solving the Ward-Tordai equation (Eqns. (2)-(3)) along with the proposed binary NP-TPeA⁺ mixture adsorption (Eqns. (13)-(16)) to give predictions of dynamic IFT.

Materials and Methods

Reagents and chemicals.

All reagents and chemicals are used as received. Potassium hydroxide (KOH, 99.9%) pellets, potassium chloride (KCl, 99.9%), 16-mercaptohexadecanoic acid (MHA, 99%), gold chloride hydrate (HAuCl₄, >49% Au), sodium borohydride (NaBH₄, >96%), tetrapentylammonium chloride (TPeACl, 99%), tetrapentylammonium hydroxide (TPeAOH, 20wt% 1 M aqueous solution) are purchased from Sigma-Aldrich. Sulfuric acid (H₂SO₄, 95.0 to 98.0 w/w %), hydrogen peroxide (H₂O₂, 30.0 to 32.0%), 2-propanol (> 99.9%), toluene (> 99.8%), NaCl salt disk, and RBS 35 Detergent Concentrate are purchased from Fisher Scientific. Deionized water (DIW, 18.2 MΩ·cm) is obtained from a Milli-Q Gradient system. All glassware, unless otherwise noted, are thoroughly cleaned with piranha solution (4:1 H₂SO₄:H₂O₂), rinsed with DIW and dried overnight in air prior to use. Synthesis, purification, and characterization of ion-pair NPs are reported in our previous work.²⁶ All experiments are performed at 295 K.

Solution conditions used to disperse NPs for all experiments.

Throughout the experiments, the ionic strength of all aqueous solutions is maintained constant at 5 mM. The pH of the aqueous phase is adjusted by mixing different ratios of 5 mM KOH/KCl, or different ratios of 5 mM TPeAOH/TPeACl. The TPeA⁺ ion concentration at a fixed aqueous pH is adjusted by mixing different ratios of pH11.0 KOH/KCl solutions and pH11.0 TPeAOH/TPeACl solutions, or mixing different ratios of pH11.7 KOH and pH11.7 TPeAOH solutions.

Dynamic interfacial tension measurements.

Dynamic interfacial tension measurements are conducted using pendant drop tensiometry. A toluene drop is formed in aqueous solutions of dispersed NPs. The IFT is monitored as soon as

the drop is formed and for over 15,000 s for the 5 nm NPs, and more than 50,000 s for the 10 nm NPs. On average the droplets volume is around 25 μL . Because the syringe, tubing, and the needle is not perfectly air-tight, decreases in the droplet volumes are observed over time. Over the whole time period of experiments, an average leakage rate of $\sim 1 \mu\text{L}/\text{hour}$ is observed, which is small compared to contributions from adsorption. All the measurements and fits of the drop shapes to the Young-Laplace equation are performed with a FTA 125 apparatus and software (First Ten Angstroms). Prior to the measurements the glass cuvette, glass syringe (2.5 mL, Model 1002 TLL SYR, Hamilton), stainless steel J-needle (20 Gauge, 304SS hub, Cadence), as well as the tubing (Fisher scientific Co.) are sonicated in 1% v/v dilute RBS solution and rinsed thoroughly with deionized water. The glass syringe, stainless steel J-needle, and the tubing were dried with N_2 and stored in toluene overnight while the glass cuvettes are stored in deionized water. Right before the measurements the cuvette is rinsed thoroughly with the gold NPs solution and the needle and tubing with toluene. All connections are sealed with Teflon tape (Fisher Scientific) first and then Parafilm (Parafilm M).

Numerical algorithm.

The Ward-Tordai equation is solved numerically following the exact procedure reported by Li *et al.*⁴⁹. In short, we use the trapezium rule of numerical integration, while the accuracy of the root finding procedure is ensured by bisection method. A step size of 1 s is used in our numerical scheme. An error of $1 \times 10^{-10} \text{ \#}/\text{nm}^2$ is allowed during the root finding scheme. A constraint is also set during the root finding so that the coverage is not allowed to exceed the maximum coverage of the species.

Results and Discussion

Adsorption isotherm for NPs

We measured the adsorption isotherms with UV-Vis spectroscopy, as described in our previous work, and shown in Figure 2.^{26, 35} We fit the measured adsorption isotherm to the Frumkin isotherm (Eqn. (4)) to obtain the equilibrium parameters ($a_{L, NP}, K_{NP}, \Gamma_{NP, \infty}$, shown in Table 1). These parameters have been discussed in our prior work are obtained independently from the dynamic IFT measurements.³⁵ Therefore, they reduce significantly the number of adjustable parameters in the analysis of dynamic surface tension measurements.

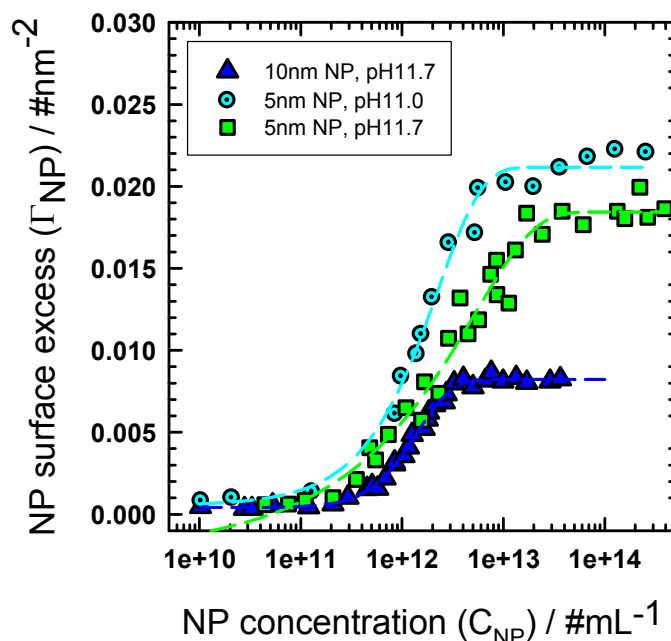


Figure 2. Adsorption isotherms of 5 nm NPs in 5 mM KOH solutions at pH 11.0 (cyan dotted circles) and pH 11.7 (green squares), as well as 10 nm NPs in 5 mM pH 11.7 KOH solution (blue triangles). Dashed lines are best fits to the Frumkin adsorption isotherm (Eqn. (4)) with fitting parameters listed in Table 1.

Table 1. Parameters for the Frumkin adsorption isotherm (Eqn. (4)) obtained from the adsorption isotherm shown in Figure 2. The relationship between the area fraction of the NPs, η_{NP} , and their surface excess, Γ_{NP} is defined by $\eta_{NP} = \Gamma_{NP} A_{NP}$, and $A_{NP} = \pi r_{NP}^2$.^a Radius of NPs consists of the core radius and the extra 1 nm representing the size of the ligand.^{26, 50}

pH	Core radius (nm)	r_{NP} (nm) ^a	$a_{L,NP}$ (#/mL)	K_{NP}	$\Gamma_{NP,\infty}$ (#/nm ²)	$\eta_{NP,\infty}$
11.0	2.5	3.5	1.6×10^{12}	0	0.022	0.85
11.7	2.5	3.5	3.1×10^{12}	-0.3	0.018	0.71
	5	6.0	2.7×10^{12}	-1.6	0.008	0.95

NP adsorption dynamics

We characterized the dynamic IFT during the adsorption of ion-pair NPs at the toluene-water interface using pendant drop tensiometry. The dynamic interfacial tension is obtained during the adsorption of NPs from the aqueous phase and shown in Figure 3. We measured the dynamic IFT during the adsorption of 5 nm NPs from an aqueous solution at pH 11.0 and at pH 11.7. We also repeated the measurements with 10 nm NPs from an aqueous solution at a pH of 11.7. For

all three cases, we varied the bulk concentrations of NPs in the aqueous phase to access equilibrium area fractions that span the full range in the measured EOS (shown in the bottom panel of Figure 3). For clarity we separated the dynamic IFT data leading to area fraction < 0.3 from those leading to higher area fractions in Figure 3 (see the EOS in the bottom panel for area fractions). We observe that the IFT decreases faster, and equilibrium IFT is lower as the NP bulk concentration increases, consistent with reported behavior of dynamic IFT for NPs (and surfactants) at the oil-water interface.^{19, 25, 51}

The equilibrium parameters are incorporated in the Ward-Tordai model (Eqn. (2)) to obtain the time-dependent surface coverage of the NPs, $\Gamma_{NP}(t)$. The diffusivities of the NPs calculated from the Stokes-Einstein equation (Eqn. (3)) are $8.6 \times 10^{-11} \text{ m}^2/\text{s}$ and $4.3 \times 10^{-11} \text{ m}^2/\text{s}$ for the 5 nm and 10 nm NPs, respectively. Finally, the wetting EOS for the NPs (Eqn. (6)) is necessary to compute the dynamic interfacial tension, and we use a core radius with an additional 1 nm for r_{NP} to account for the surface functional groups.²⁶ The corresponding measured EOS is shown in the bottom row of Figure 3, where the red solid lines represent the wetting EOS (Eqn. (6)). As discussed previously, the data deviates from the predictions of Eqn. (6) at higher coverage. We suspect that these deviations are due to polydispersity, where the average NP radius contributing to the equilibrium pressure is smaller at higher coverage.³⁵ The insets in the EOS show the effective radii corresponding to each equilibrium pressure, which is obtain from $r_{eff} = r_{NP} \sqrt{\Pi_{NP} / \gamma_{OW} \eta_{NP}}$. When fitting the dynamic IFT we use the effective radii obtained from the EOS for all concentrations.

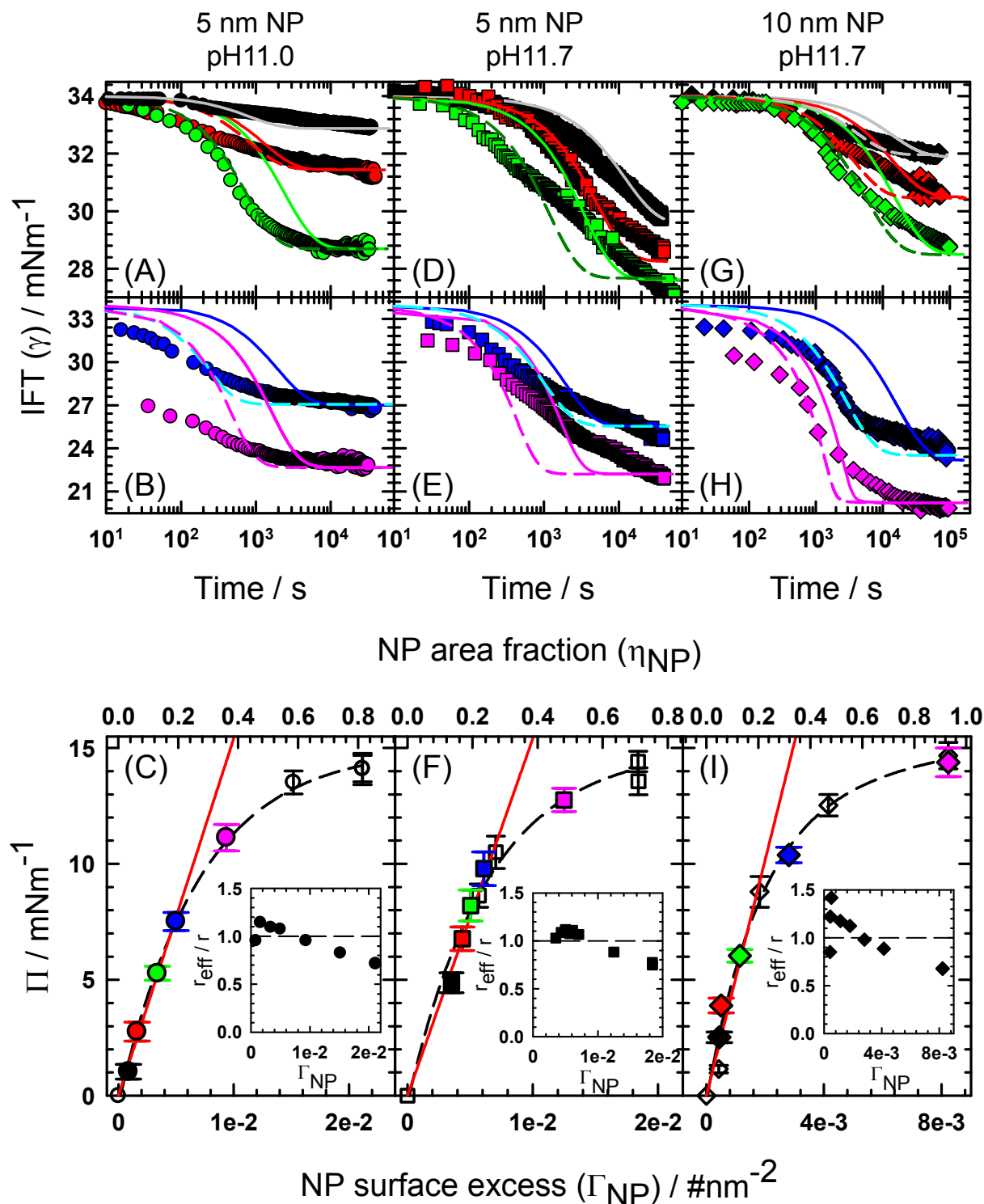


Figure 3. Dynamic interfacial tension of (A,B) 5 nm NPs in pH 11.0 solution with NP concentrations of 3.5×10^{10} /mL (black), 1.2×10^{11} /mL (red), 3.5×10^{11} /mL (green), 5.5×10^{11} /mL (blue), and 1.5×10^{12} /mL (pink); (D,E) 5 nm NP in pH 11.7 solution with NP concentrations of 4.7×10^{11} /mL (black), 6.4×10^{11} /mL (red), 8.5×10^{11} /mL (green), 1.2×10^{12} /mL (blue), and 5.6×10^{12} /mL (pink); and (G,H) 10 nm NP in pH 11.7 solution, with NP concentrations of

6.3×10^{10} /mL (black), 1.2×10^{11} /mL (red), 3.7×10^{11} /mL (green), 8.0×10^{11} /mL (blue), 9.0×10^{12} /mL (pink). For the first two rows, the solid lines are predictions from Eqns. (2)-(7), with parameters listed in Table 1, and dashed lines are using the diffusivity as an adjustable parameter. The measured EOS for the NPs are shown for (C) 5 nm NPs at pH 11.0 (F) 5 nm NPs at pH 11.7, and (I) 10 nm NP at pH 11.7. The color of the solid data points in (C), (F), and (I) corresponds to each dynamic interfacial tension data shown in the upper panels. Insets of (C), (F), and (I) are the calculated size based on Eqn. (6). Hollow points are extra measurements of pressure isotherms. For all measurements the ionic strength is 5 mM.

The measured dynamic IFT is well-described with the proposed model, as shown from the solid lines of Figure 3. Note that *no fitting parameters* are used when comparing the dynamic IFT to the model. The surface pressure reached at long time is predicted with equilibrium parameters obtained from independently measured adsorption isotherm (Figure 2). In general, the model captures well the diffusion-limited dynamics and equilibration time for area fraction lower than ~ 0.3 ($\theta_{NP} \sim 0.45$). The agreement between the data and the model demonstrates that the treatment for NP adsorption is different from that of surfactant due to the presence of the wetting EOS. In fact, relying solely on the Frumkin adsorption isotherm and its associated EOS (ignoring the wetting contribution) would not lead to a measurable decrease in IFT, see the black dashed lines in Figure 4.

Unfortunately, we cannot rule out that some amount of convection might be present in our measurements. In particular, measurements in the adsorption regime of Figure 3 shows a slightly faster decrease in the IFT than what we expect. If we allow the diffusivity of the NPs to vary we see that a slight increase in the diffusivity leads to a much better agreement between the experiments and the model, as shown by the dashed line in Figure 4 for the 5 nm and 10 nm NPs. We find that using diffusivity as a fitting parameter (D_{eff}), rather than directly applying the predicted value from Stokes-Einstein model is the only effective way to better capture the dynamic interfacial tension during the adsorption period (*i.e.*, around 100 s to 1000 s). Note that the parameters from the Frumkin equation are obtained independently from the adsorption isotherm. An extensive parameter space exploration, shown in Supporting Information Figures S1-S2, plots how all the other parameters would affect the predicted curves, show that varying the other parameters would not lead to a better agreement. The predictions using the diffusivity as an adjustable parameter that gives a better agreement in the adsorption regime are also shown

in Figure 3, and the corresponding values for the diffusivities are shown in Supporting Information Figure S3. Polydispersity of the NPs should also be considered as another possible explanation for a faster adsorption. In particular, Schwenke *et al.*²⁷ clearly showed that when polydispersity of the bulk dispersion increases, faster adsorption could be observed compared to a less polydispersed bulk dispersion, although similar equilibrium coverage could be reached, likely due to the replacement of small NPs by large NPs at longer times.⁵²

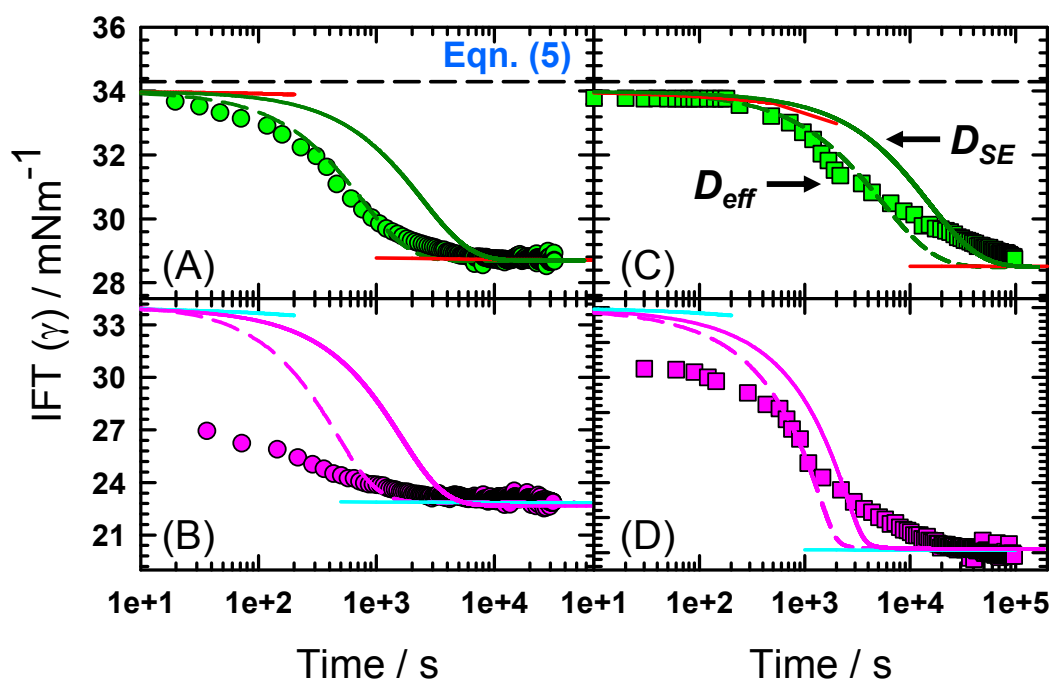


Figure 4. Effect of using the diffusivity as an adjustable parameter in Eqn. (2) for (A) 5 nm NP with concentration of 3.5×10^{11} /mL (green circle), and 1.5×10^{12} /mL (pink circle) in 5mM pH 11.0 and for (B) 10 nm NP with concentration of 3.7×10^{11} /mL (green square), and 9.0×10^{12} /mL (pink square). Solid lines are predictions using diffusivity estimated from Stokes-Einstein equation (Eqn. (3)). Dark green and pink dashed lines are predictions using the diffusivity as an adjustable parameter, with a diffusivity 2.5 fold larger. The black dashed lines is the dynamic IFT predicted by using Frumkin EOS (Eqn. (5)) without the wetting EOS. Asymptotic limits (Eqn. (9) and Eqn. (11)) are shown in solid lines, with red solid lines corresponding to the low concentration cases and cyan solid lines corresponding to high concentration cases.

In general, when we increase the bulk NP concentration and reach higher area fractions (middle row in Figure 3) we predict shorter equilibration time than what is measured experimentally. In terms of a slow equilibration time, Schwenke *et al.*²⁷ also showed that local ordering processes directly affect the adsorption at high surface coverage, which slows down the adsorption and thus the decrease in interfacial tension. Moreover, Luu *et al.*⁵³ conducted

dissipative particle dynamics simulations and found out that as surface coverage increases, the self-diffusion coefficient decreases quickly due to caging effects. Kaz *et al.*⁵⁴ also observed an extremely slow relaxation time for single micron-sized particle. In addition, recent experiments by Huerre *et al.*⁵⁵ indicate that re-organization within the interface happens during the late stage of adsorption. Finally, Bizmark proposed that an adsorption barrier might be present at later stages of the adsorption process, when the particles have reached a high coverage.¹⁹ For an energy barrier between the bulk and the interface to affect the adsorption kinetics, the time scale associated with the energy barrier has to be slower than the time scale associated with diffusion. Alvarez *et al.*⁵⁶ provided an estimate for the relative kinetic time scale, τ_k , as well as the diffusion time scale, τ_D .³⁶ The estimated diffusion time scale is on the order of $10^2 - 10^3$ seconds depending on NP concentrations. The kinetic time scale, which depends on adsorption and desorption rate constant, is harder to estimate. However, unless the kinetic time scale is slower than the diffusion time scale, it is difficult to observe the kinetic limitations with pendant drop tensiometry.^{11, 56} The scaling arguments of Alvarez *et al.* also indicate that in most cases dynamic IFT measurements using a pendant drop would not be affected by the presence of an energy barrier between the bulk and the interface.^{11, 56}

We estimate the asymptotic limits using Eqn. (9) for short-time and Eqn. (11) for long-time, with parameters listed in Table 1. As shown by the solid lines in Figure 4, both limits agree well with the full Ward-Tordai model using the same parameters as the ones listed in Table 1. Due to data acquisition limitations, the short-time limit does not agree well the experimental measurements at high concentration. The predicted long-time limits for different NP concentration and for the two NP sizes are shown in Figure 5. Also shown are the predictions for the full Ward-Tordai model. The slopes for the 10nm NPs (Figure 5B) are smaller compared to those obtained with the 5nm NPs (Figure 5A). In addition, the time window where the long-time limit agrees with the full solution is longer for large particles compared to the small particles. It is consistent with slower diffusion of large NPs.^{19, 31}

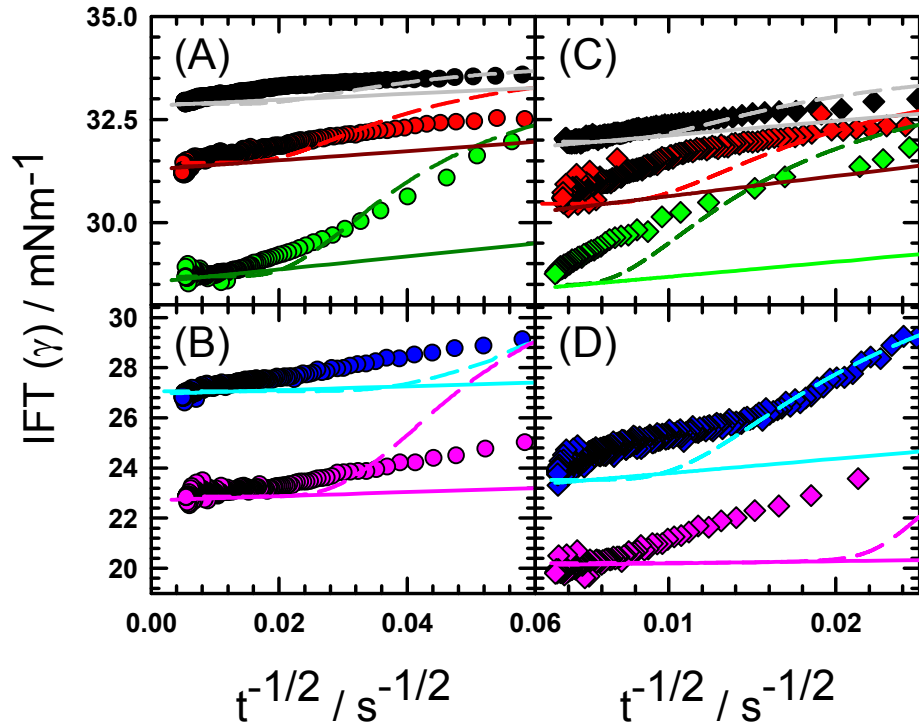


Figure 5. Long-time limits of (A, B) 5 nm NPs in pH 11.0 aqueous solution with NP concentrations of 3.5×10^{10} /mL (black), 1.2×10^{11} /mL (red), 3.5×10^{11} /mL (green), 5.5×10^{11} /mL (blue), and 1.5×10^{12} /mL (pink); (C, D) 10 nm NP in pH 11.7 solution, with NP concentrations of 6.3×10^{10} /mL (black), 1.2×10^{11} /mL (red), 3.7×10^{11} /mL (green), 8.0×10^{11} /mL (blue), 9.0×10^{12} /mL (pink). Points are experimental measurements, dashed lines are full solutions of the Ward-Tordai model, and the solid lines are long-time limits obtained from Eqn. (11) with parameters listed in Table 1. For all measurements the ionic strength is 5 mM.

The full prediction of the diffusion-limited adsorption dynamics enables a comparison of the adsorption rate between experimental measurements and theoretical predictions. For the data we can readily convert the instantaneous surface pressure into a dynamic surface excess, $\Gamma(t)$, using Eqn. (6). From these data we can also obtain the experimental adsorption rate, $d\Gamma/dt$. We can follow the same procedure for the predictions of the Ward-Tordai model. Shown in Figure 6 are the measured adsorption rate of 5 nm NPs and 10 nm NPs as a function of surface excess (and area fraction) that we compare to the predictions obtained from the Ward-Tordai model (dashed lines). We see that the experimental adsorption rate is faster at lower coverage (<1000 sec) compared to predictions, either due to polydispersity (small NPs diffuse faster) or convection (or both).²⁷ As the surface excess of NP increases, the measured adsorption rate fluctuates around

the theoretical predictions, but we cannot rule out longer equilibration times caused by particle re-arrangement within the interface as the surface coverage increases.⁵⁵

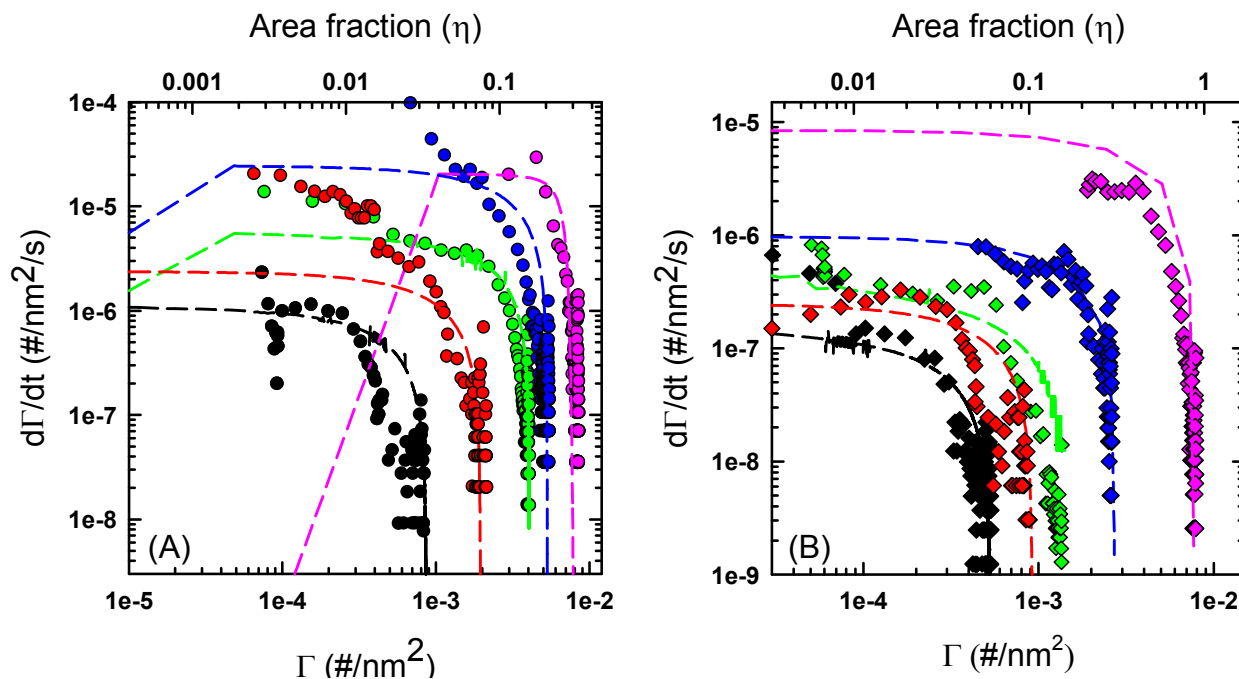


Figure 6. Adsorption rate of (A) 5 nm NPs in pH 11.0 solution with NP concentrations of 3.5×10^{10} /mL (black), 1.2×10^{11} /mL (red), 3.5×10^{11} /mL (green), 5.5×10^{11} /mL (blue), and 1.5×10^{12} /mL (pink); (B) 10 nm NP in pH 11.7 solution, with NP concentrations of 6.3×10^{10} /mL (black), 1.2×10^{11} /mL (red), 3.7×10^{11} /mL (green), 8.0×10^{11} /mL (blue), 9.0×10^{12} /mL (pink). Points are obtained from experimental measurements, dashed lines are adsorption rate predicted from full dynamic fittings with diffusivity used as an adjustable parameter (dashed lines in Figure 3). For all measurements the ionic strength is 5 mM.

Competitive adsorption of NP-ion mixture

We test if the proposed dynamic model can be extended to study the diffusion-limited competitive adsorption between the NPs and a surface active species (here the TPeA⁺ which is also present as a ligand on the NPs). Introducing a surface active species allows us to modulate the surface pressure contributions captured by the Frumkin EOS (Eqn. (15)) so that it is no longer negligible. We first characterize the dynamic IFT for the adsorption of TPeA⁺ to the oil-water interface in the absence of NPs (Figure 7). The dynamic IFT measurements are performed in solutions with a total ionic strength of 5 mM, and at pH 11.0 and pH 11.7. A radius of 0.5 nm is assumed for the TPeA⁺ ion⁵⁰ yielding a diffusivity of 4.3×10^{-10} m²/s using Eqn. (3). The

thermodynamic parameters obtained from the equilibrium pressure isotherm are listed in Table 2 (the equilibrium data is also shown in Supporting Information, Figure S4). We find that the dynamic IFT is well-described by the Ward-Tordai model. Here we adjust the diffusivity slightly from D_{SE} (Figure 7C). We observe that the diffusivity of TPeA⁺ decreases slightly as the bulk concentration of TPeA⁺ increases, likely due to existence of adsorption energy barrier as surface coverage increases.¹⁷ Similar results have been reported for the adsorption of surfactants.^{16, 17}

Table 2. Parameters for the TPeA⁺ adsorption at pH 11.0 and pH 11.7 obtained from fitting equilibrium pressure isotherms to Frumkin model, Eqns. (4)-(5).

pH	$a_{L,I}$ (mM)	K_I	$\Gamma_{I,\infty}$ (#/nm ²)	$\eta_{I,\infty}$
pH 11.0	1.0×10^{-6}	6.0	0.204	0.160
pH 11.7	2.5×10^{-7}	6.6	0.207	0.163

Dynamic IFT measurements for binary mixtures of NPs and TPeA⁺ are shown in Figure 8. Here the TPeA⁺ bulk concentration is maintained at 0.01 mM, while NP bulk concentration is varied across 2 orders of magnitude. Because we characterized the dynamic IFT for the single components (Figure 3 and Figure 7), all the equilibrium adsorption parameters for the single components are available (listed in Table 1 and Table 2). For the binary mixture, an additional parameter is necessary to account for the NP-TPeA⁺ interactions within the interface in the binary Frumkin model (Eqns. (13)-(15)). In our previous work,³⁵ we obtained the equilibrium EOS and found that the best fit for the interaction parameter in the binary Frumkin equations was $K_{NP-I} = -7$, making all equilibrium parameters available to predict the dynamic IFT for the case of competitive adsorption. To compare with the experimental data, we use diffusivities calculated from Stokes-Einstein equation for each species. The predicted dynamic IFT are shown as the solid lines in Figure 8A and C. The lines are obtained by solving the Ward-Tordai equation for two species simultaneously, along with the binary Frumkin adsorption isotherm as well as the binary Frumkin EOS and the wetting EOS for the NPs. We highlight the fact that lines in Figure 8 are obtained without adjustable parameters. As shown, the predictions show qualitative agreement with the data and the observed equilibration time for NP area fractions up to ~0.1 (Figure 8A). Similar to what we observe for the pure NPs, we find that at high NP bulk

concentration, a shorter equilibration time is predicted compared to the experimental data, where slower dynamic is observed.

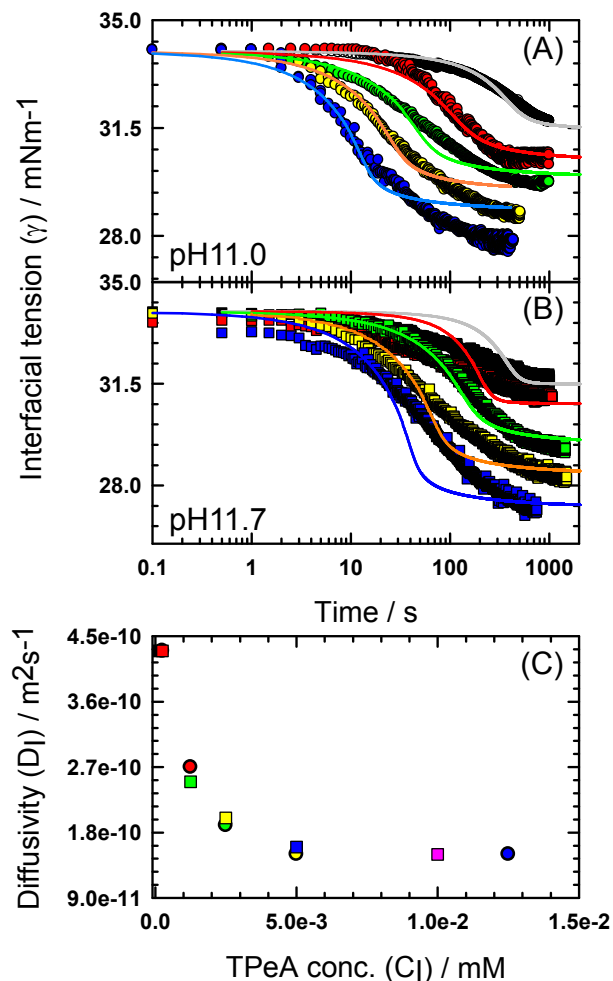


Figure 7. Dynamic IFT of TPeA⁺ ions in 5 mM solutions at (A) pH 11.0 with TPeA⁺ concentrations of 2.5×10^{-4} mM (black), 1.25×10^{-3} mM (red), 2.5×10^{-3} mM (green), 5×10^{-3} mM (yellow), 1.25×10^{-2} mM (blue), and at (B) pH 11.7 with TPeA⁺ concentrations of 1.25×10^{-4} mM (black), 2.5×10^{-4} mM (red), 1.25×10^{-3} mM (green), 2.5×10^{-3} mM (yellow), 1×10^{-2} mM (blue). Solid lines are fitting to Ward-Tordai model (Eqn. (2)) combined with Frumkin model (Eqns. (4)-(5)). The corresponding diffusivity used is shown in (C) with corresponding colored circle representing diffusivity at pH 11.0 and corresponding colored squares representing diffusivity at pH 11.7.

hydroxypropylmethylcellulose and octanesulfonic acid sodium salt mixture as well.⁵⁸ Moreover, it is consistent with our previous work³⁵ on the competition between NP and TPeA⁺ ion for the interface. A few parameters could be adjusted to improve the agreement with the experimental data. However, the coverage of TPeA⁺ within the interface is extremely close to its maximum coverage, making it numerically challenging to perform a parametric study.

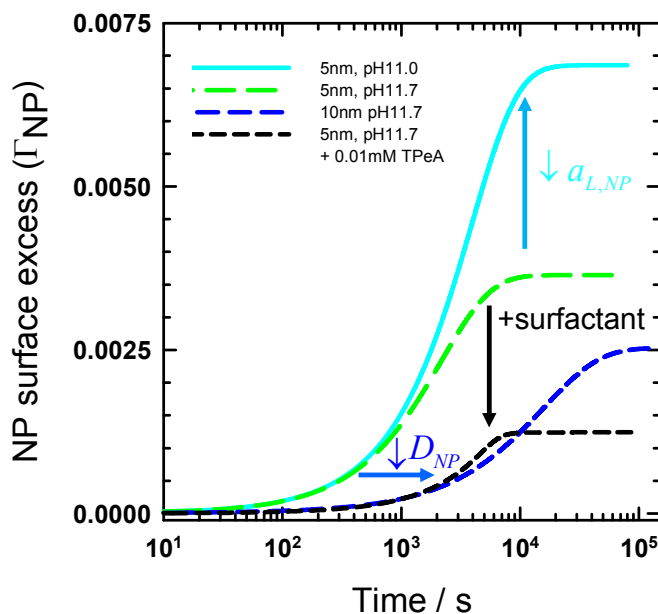


Figure 9. Evolution of the surface coverage for 5 nm NPs at pH11.0 solution (cyan solid line), 5 nm NP at pH11.7 solution (green long dashed line), 10 nm NP at pH11.7 solution (blue medium dashed line), 5 nm NP in the presence of 0.01 mM TPeA⁺ (black short dashed line) at a bulk concentration of 7.5×10^{11} /mL.

Based on the dynamic model proposed and its agreement with experimental data we can highlight how the individual thermodynamic parameters ($a_{L,NP}$, K_{NP} , $\Gamma_{NP,\infty}$, $a_{L,I}$, K_I , $\Gamma_{I,\infty}$, K_{NP-I}) affect the instantaneous and equilibrium surface excess of the NPs at the interface (Figure 9). First, consider the differences in the dynamic surface excess between the two pHs for the adsorption of 5 nm NPs (cyan solid line for 5 nm NP dispersed in pH 11.0 solution and green long dashed line for 5 nm NP dispersed in pH 11.7 solution in Figure 9). The only significant difference between the two curves is the smaller dissociation constant for the particles in a pH11.0 solution (the particles have the same size, therefore the same diffusivity). We see that initially the coverage is identical, but as the adsorption process proceeds the NPs in pH 11.0 have a higher surface excess than the NPs in pH 11.7. Then, a comparison between the 5 nm and 10

nm in pH 11.7 illustrates the case where the dissociation constant is similar, but the diffusivity for the smaller particles is larger. As a result, we see that initially the small NPs adsorb to the interface faster, but over time a higher area fraction is obtained for the larger NPs. Finally, competitive adsorption due to the presence of a surfactant leads to a lower NP coverage at all times, even if the dissociation constant and diffusivity for the NPs remain the same (green and black line in Figure 9).

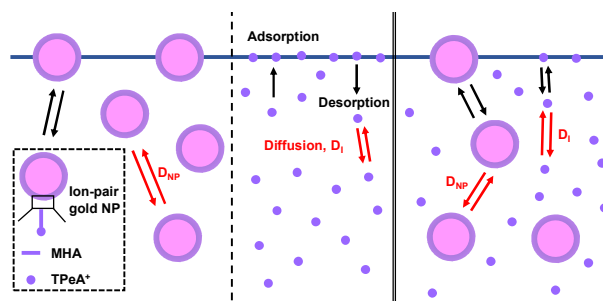
Conclusions

We measured dynamic interfacial tension of NPs, TPeA⁺ ions, and NP-TPeA⁺ ion mixtures at toluene-water interface. We obtain predictions for dynamic interfacial tension of the three different systems based on the Ward-Tordai model, the Frumkin adsorption isotherm, and the addition of a wetting contribution for the NPs. We also derive the long-time limit for diffusion-limited NP adsorption. We demonstrate that the Ward-Tordai model can be employed to describe the diffusion-limited adsorption of NPs to a fluid interface, and deviations from the model can be employed to uncover other rate-limiting mechanisms. Good agreement is reached at low NP bulk concentrations, where some deviations are observed at high NP bulk concentration. We suspect that deviations in this regime are likely due to convection or polydispersity of the NPs causing an apparent faster adsorption after the induction period. Slower dynamics at the late stages of adsorption could arise due to NP re-arrangement within the interface or the existence of energy barriers when interfacial coverage is high. This proposed method of modeling dynamic adsorption reduces the complexity of analyzing short time and long time asymptotic behaviors, which can be plagued by low resolution and are not applicable at high NP concentrations. In addition, deviations from this simple model open the door to quantify other more complex effects occurring at the interface such as polydispersity or relaxation. Finally, the modeling approach reported in this work was extended to describe binary competitive adsorption of NP-surfactant mixtures.

Acknowledgements

This work is partially supported by the National Science Foundation (CBET-1510671 and CBET-1436482), the Donors of the American Chemical Society Petroleum Research Fund (51803-ND5), and the Air Force Office of Scientific Research (FA9550-12-1-0090).

Table of Content



References

1. J. Lacava, A.-A. Ouali, B. Raillard and T. Kraus, *Soft Matter*, 2014, **10**, 1696-1704.
2. J. Tang, P. J. Quinlan and K. C. Tam, *Soft Matter*, 2015, **11**, 3512-3529.
3. Y. Zhu, T. Fu, K. Liu, Q. Lin, X. Pei, J. Jiang, Z. Cui and B. P. Binks, *Langmuir*, 2017, **33**, 5724-5733.
4. Z. Chen, L. Zhou, W. Bing, Z. Zhang, Z. Li, J. Ren and X. Qu, *J. Am. Chem. Soc.*, 2014, **136**, 7498-7504.
5. E. Smirnov, P. Peljo, M. D. Scanlon and H. H. Girault, *ACS Nano*, 2015, **9**, 6565-6575.
6. A. N. Shipway, E. Katz and I. Willner, *ChemPhysChem*, 2000, **1**, 18-52.
7. Y. H. Lee, W. Shi, H. K. Lee, R. Jiang, I. Y. Phang, Y. Cui, L. Isa, Y. Yang, J. Wang, S. Li and X. Y. Ling, *Nat. Commun.*, 2015, **6**, 6990.
8. P.-P. Fang, S. Chen, H. Deng, M. D. Scanlon, F. Gumy, H. J. Lee, D. Momotenko, V. Amstutz, F. Cortés-Salazar, C. M. Pereira, Z. Yang and H. H. Girault, *ACS Nano*, 2013, **7**, 9241-9248.
9. Y. Montelongo, D. Sikdar, Y. Ma, A. J. S. McIntosh, L. Velleman, Anthony R. Kucernak, J. B. Ediel and A. A. Kornyshev, *Nat. Mater.*, 2017, **16**, 1127.
10. B. P. Binks, *Curr. Opin. Colloid Interface Sci.*, 2002, **7**, 21-41.
11. N. J. Alvarez, W. Lee, L. M. Walker and S. L. Anna, *J. Colloid Interface Sci.*, 2011, **355**, 231-236.
12. K. Du, E. Glogowski, T. Emrick, T. P. Russell and A. D. Dinsmore, *Langmuir*, 2010, **26**, 12518-12522.
13. Y. Zhang, S. Wang, J. Zhou, R. Zhao, G. Benz, S. Tcheimou, J. C. Meredith and S. H. Behrens, *Langmuir*, 2017, **33**, 4511-4519.
14. D. Langevin, *Curr. Opin. Colloid Interface Sci.*, 1998, **3**, 600-607.
15. J. S. Erickson, S. Sundaram and K. J. Stebe, *Langmuir*, 2000, **16**, 5072-5078.
16. J. Eastoe, J. S. Dalton and R. K. Heenan, *Langmuir*, 1998, **14**, 5719-5724.
17. J. Eastoe and J. S. Dalton, *Adv. Colloid Interface Sci.*, 2000, **85**, 103-144.
18. R.-Y. Tsay, T.-F. Wu and S.-Y. Lin, *J. Phys. Chem. B*, 2004, **108**, 18623-18629.
19. N. Bizmark, M. A. Ioannidis and D. E. Henneke, *Langmuir*, 2014, **30**, 710-717.

20. Y. Han, N. Bizmark, N. M. Abukhdeir and M. A. Ioannidis, *Phys. Chem. Chem. Phys.*, 2017, **19**, 24955-24960.
21. C. E. Colosqui, J. F. Morris and J. Koplik, *Phys. Rev. Lett.*, 2013, **111**, 028302.
22. A. F. H. Ward and L. Tordai, *J. Chem. Phys.*, 1946, **14**, 453-461.
23. S. Simovic and C. A. Prestidge, *Langmuir*, 2004, **20**, 8357-8365.
24. M. Wang, Z. Zhang and J. He, *Langmuir*, 2015, **31**, 12911-12919.
25. C. Stefaniu, M. Chanana, D. Wang, D. V. Novikov, G. Brezesinski and H. Möhwald, *Langmuir*, 2011, **27**, 1192-1199.
26. X. Hua, M. A. Bevan and J. Frechette, *Langmuir*, 2016, **32**, 11341-11352.
27. K. Schwenke, L. Isa and E. Del Gado, *Langmuir*, 2014, **30**, 3069-3074.
28. N. Bizmark and M. A. Ioannidis, *Langmuir*, 2015, **31**, 9282-9289.
29. V. B. Fainerman, A. V. Makievski and R. Miller, *Colloids Surf., A*, 1994, **87**, 61-75.
30. R. Van den Bogaert and P. Joos, *The Journal of Physical Chemistry*, 1980, **84**, 190-194.
31. A. Nelson, D. Wang, K. Koynov and L. Isa, *Soft Matter*, 2015, **11**, 118-129.
32. G. Zhang and S. Torquato, *Physical Review E*, 2013, **88**, 053312.
33. N. J. Alvarez, S. L. Anna, T. Saigal, R. D. Tilton and L. M. Walker, *Langmuir*, 2012, **28**, 8052-8063.
34. M. Luo, G. K. Olivier and J. Frechette, *Soft Matter*, 2012, **8**, 11923-11932.
35. X. Hua, M. A. Bevan and J. Frechette, *Langmuir*, 2018, doi: 10.1021/acs.langmuir.8b00053
36. N. J. Alvarez, L. M. Walker and S. L. Anna, *Langmuir*, 2010, **26**, 13310-13319.
37. J. K. Ferri and K. J. Stebe, *Colloids Surf., A*, 1999, **156**, 567-577.
38. R. C. Daniel and J. C. Berg, *J. Colloid Interface Sci.*, 2003, **260**, 244-249.
39. R. Miller, V. B. Fainerman, E. V. Aksenenko, M. E. Leser and M. Michel, *Langmuir*, 2004, **20**, 771-777.
40. V. B. Fainerman, M. Lotfi, A. Javadi, E. V. Aksenenko, Y. I. Tarasevich, D. Bastani and R. Miller, *Langmuir*, 2014, **30**, 12812-12818.
41. S.-Y. Lin, K. McKeigue and C. Maldarelli, *AIChE J.*, 1990, **36**, 1785-1795.
42. J. T. Edward, *J. Chem. Educ.*, 1970, **47**, 261.
43. V. L. Kolev, K. D. Danov, P. A. Kralchevsky, G. Broze and A. Mehreteab, *Langmuir*, 2002, **18**, 9106-9109.
44. A. J. Prosser and E. I. Franses, *Colloids Surf., A*, 2001, **178**, 1-40.
45. S. Sundaram, J. K. Ferri, D. Vollhardt and K. J. Stebe, *Langmuir*, 1998, **14**, 1208-1218.
46. W. R. Gillap, N. D. Weiner and M. Gibaldi, *J. Phys. Chem.*, 1968, **72**, 2222-2227.
47. J. C. Berg, *An Introduction to Interfaces and Colloids: The Bridge to Nanoscience*, World Scientific Publishing Co. Pte. Ltd., 2009.
48. V. B. Fainerman, N. Mucic, V. Pradines, E. V. Aksenenko and R. Miller, *Langmuir*, 2013, **29**, 13783-13789.
49. X. Li, R. Shaw, G. M. Evans and P. Stevenson, *Comput. Chem. Eng.*, 2010, **34**, 146-153.
50. G. K. Olivier, D. Shin, J. B. Gilbert, L. M. A. Monzon and J. Frechette, *Langmuir*, 2009, **25**, 2159-2165.
51. S. Kutuzov, J. He, R. Tangirala, T. Emrick, T. P. Russell and A. Boker, *Phys. Chem. Chem. Phys.*, 2007, **9**, 6351-6358.
52. Y. Lin, H. Skaff, T. Emrick, A. D. Dinsmore and T. P. Russell, *Science*, 2003, **299**, 226-229.
53. X.-C. Luu, J. Yu and A. Striolo, *Langmuir*, 2013, **29**, 7221-7228.
54. D. M. Kaz, R. McGorty, M. Mani, M. P. Brenner and V. N. Manoharan, *Nat. Mater.*, 2011, **11**, 138.
55. A. Huerre, F. Cacho-Nerin, V. Poulichet, C. E. Udoh, M. De Corato and V. Garbin, *Langmuir*, 2018, **34**, 1020-1028.
56. N. J. Alvarez, L. M. Walker and S. L. Anna, *Physical Review E*, 2010, **82**, 011604.
57. M. Mulqueen, S. S. Datwani, K. J. Stebe and D. Blankshtein, *Langmuir*, 2001, **17**, 7494-7500.
58. A. Avranas and P. Iliou, *J. Colloid Interface Sci.*, 2003, **258**, 102-109.

